

Comparing Hydroxyl Terminated Polybutadiene and Acrylonitrile Butadiene Styrene as Hybrid Rocket Fuels

Stephen A. Whitmore,* Zachary W. Peterson,† and Shannon D. Eilers†
Utah State University, Logan, Utah 84322

DOI: 10.2514/1.B34382

Acrylonitrilebutadiene-styrene thermoplastic, widely mass-produced for noncombustion applications including household plumbing and structural materials, is evaluated and compared with hydroxyl-terminated polybutadiene as a potential fuel for hybrid rocket motors. Acrylonitrilebutadiene-styrene has several mechanical properties, including its ability to be fabricated into a wide variety of shapes using fused deposition modeling, which are very attractive as a potential hybrid rocket fuel. The acrylonitrilebutadiene-styrene grains were fabricated using fused deposition modeling from existing rapid-prototyping stock materials composed of 50:43:7 butadiene, acrylonitrile, and styrene mole fractions. The acrylonitrilebutadiene-styrene grains were burned with nitrous oxide as the matching oxidizer and compared for performance and consistency against fuel grains of equal size cast from hydroxyl-terminated polybutadiene and burned with nitrous oxide. Test results demonstrate a higher burn-to-burn consistency for acrylonitrilebutadiene-styrene, but slightly reduced overall performance. Methods for increasing the burn energy of the acrylonitrilebutadiene-styrene fuel grains were investigated. Equilibrium chemistry calculations conclude that, for a given oxidizer-to-fuel ratio, varying the butadiene mole fraction in the acrylonitrilebutadiene-styrene formulation has a significant effect on the propellant performance. A major result of this research is the demonstrated viability of thermoplastic as a hybrid rocket fuel grain material.

Nomenclature

A_{burn}	= fuel grain surface burn area, cm^2
A_c	= fuel chamber cross-sectional area, cm^2
A_{exit}	= nozzle exit area, cm^2
A_{ox}	= effective total oxidizer injector area, cm^2
A^*	= nozzle throat area, sonic choke area, cm^2
C	= carbon atom
C_{dox}	= effective oxidizer injector discharge coefficient
C_p	= specific heat of combustion products, $\text{J/kg} \cdot \text{K}$
c^*	= propellant characteristic velocity, m/s
D_{final}	= final port diameter, cm
D_0	= initial port diameter, cm
F	= steady-state thrust, N
\bar{G}_{ox}	= mean oxidizer mass flux $\text{kg/s} \cdot \text{cm}^2$
H	= hydrogen atom
h_v	= heat of ablation/gasification, MJ/kg
I_{sp}	= specific impulse, s
L	= fuel grain port length, cm
M_W	= molecular weight of combustion products
\dot{m}_{fuel}	= solid fuel grain mass flow rate, kg/s
\dot{m}_{ox}	= oxidizer mass flow rate, kg/s
N	= degree of polymerization
P_{ox}	= oxidizer injector upstream feed pressure, kPa
P_r	= Prandtl number
P_0	= combustion chamber pressure, kPa
R_g	= gas-specific constant, $\text{J/kg} \cdot \text{K}$
\dot{r}	= fuel grain linear regression rate, cm/s

Presented as Paper 2011-8195 at the 47th AIAA/ASME/SAE/ASEE Joint Propulsion Conference & Exhibit, San Diego, CA, 31–3 August 2011; received 30 June 2011; revision received 11 June 2012; accepted for publication 12 September 2012; published online 5 April 2013. Copyright © 2012 by Utah State University. Published by the American Institute of Aeronautics and Astronautics, Inc., with permission. Copies of this paper may be made for personal or internal use, on condition that the copier pay the \$10.00 per-copy fee to the Copyright Clearance Center, Inc., 222 Rosewood Drive, Danvers, MA 01923; include the code 1533-3876/13 and \$10.00 in correspondence with the CCC.

*Associate Professor, Mechanical and Aerospace Engineering Department, 4130 Old Main Hill, UMC 4130. Associate Fellow AIAA.

†Graduate Research Assistant, Mechanical and Aerospace Engineering Department, 4130 Old Main Hill, UMC 4130. Student Member AIAA.

\bar{r}_{dia}	= mean regression rate based on mean port diameter and burn time, cm/s
\bar{r}_{mass}	= mean regression rate based consumed mass and burn time, cm/s
T_0	= adiabatic flame temperature, K
t_{burn}	= burn time, s
V_c	= combustion chamber internal volume, cm^3
γ	= ratio of specific heats or combustion products
ΔG	= Gibbs free energy of formation, kJ/mol
ΔH	= mole-specific enthalpy change, kJ/mol
ΔH_f^0	= standard enthalpy of formation, kJ/mol
ΔM_{fuel}	= consumed fuel mass, kg
ΔM_{ox}	= consumed oxidizer mass, kg
ΔQ_c	= heat of combustion, kJ/mol
ΔQ_{poly}	= heat of polymerization, kJ/mol
η^*	= combustion efficiency
μ	= dynamic viscosity, $\text{Nt} \cdot \text{s/m}^2$
ρ_{fuel}	= solid fuel grain material density, kg/m^3
ρ_{ox}	= liquid oxidizer density, kg/m^3

I. Introduction

DURING the past 50 years, conventional launch systems have been developed to a high state of capability; however, for a variety of reasons, these vehicles have become increasingly expensive to operate. Some of these reasons include manufacturing and operational complexity, safety, and environmental regulations for dealing with hazardous materials, and the generally large “support army” required for flight preparations. Because of high launch performance demands, including specific impulse I_{sp} and thrust-to-weight ratio, conventional liquid- and solid-propelled rocket stages that employ highly energetic, explosive, or toxic propellants will likely remain the systems of choice for large military-class payloads or for human spaceflight. However, there exists an emerging commercial market that is willing to accept a lower system performance in exchange for reduced operational costs and lower environmental impact.

Hybrid motors that employ nontoxic, nonexplosive propellants have the potential to fulfill this “market niche.” Although hybrid systems generally deliver lower I_{sp} than conventional bipropellant liquid and solid rockets of the same thrust level, because the

propellant components remain inert until ignited within the motor chamber, hybrid rockets are inherently safer to transport, load, store, and operate [1]. This inherent safety greatly reduces ground handling and transportation costs and can potentially lead to an overall reduction in system operating costs. Unlike solid-propelled rockets, where fuel grain flaws and age-induced cracks present a significant safety issue, hybrid rockets exhibit a relative insusceptibility to grain flaws. Other advantages of hybrid rockets that can potentially offset the lower performance level include the ability to be restarted in flight and the ability to be throttled over a significantly wider range of thrust levels than conventional liquid bipropellant systems. Hybrid propelled rocket stages are especially attractive for micro- or nanosatellite scale launch vehicles, where high thrust-to-weight ratios are not required. For nanosat launch systems, the ballistic coefficients are significantly lower compared with conventional launch vehicles; consequently, trajectories that are optimized for large-scale launch systems may not necessarily be suitable.

Hybrid rocket motors have been in development for more than two decades, but have seen little commercial application, mainly due to difficulty associated with mass producing fuel grains. The current production method involves casting viscous or nonpolymerized material “by hand” in a casing mold to form the fuel grain, to be later manually assembled with other motor components, including the igniter, oxidizer tank, valves and injectors, pre- and postcombustion chambers, and the rocket nozzle. This low-tech manufacture and assembly approach results in market prohibitive production costs and cannot produce the numbers and varieties of motors required to support the ambitious launch rates necessary to support what is expected to be a fast-growing commercial space industry.

Leveraging the recent rapid capability growth in factory automation and robotics, a type of direct-digital manufacturing known as fused deposition modeling (FDM) [2] offers the potential to revolutionize previous methods used to fabricate hybrid rocket fuel grains. FDM manufacturing, also commonly known as “rapid prototyping,” works on an additive-fabrication principle by laying down material in layers. A plastic filament is unwound from a coil and supplies material to an extrusion nozzle. The nozzle is heated to melt the material and is moved in both horizontal and vertical directions by a computer numerically controlled (CNC) mechanism. This manufacturing method can support high production rates and offers the potential of improving hybrid fuel grain quality, consistency, and performance, while reducing development and production costs.

II. Acrylonitrile Butadiene Styrene as a Hybrid Rocket Fuel Alternative to Hydroxyl-Terminated Polybutadiene

The most commonly used hybrid rocket fuel, hydroxyl-terminated polybutadiene (HTPB) is a legacy thermosetting polymer material frequently used as a binder for solid-rocket propellant grains. It remains the hybrid fuel grain material of choice primarily because of industry familiarity with its chemical and structural properties. HTPB is a solid homopolymer made by combining two components: 1) a hydroxyl-terminated polymer of butadiene and 2) a cross-linking agent, either isocyanate or methylene diphenyl diisocyanate (MDI), used to polymerize and set the material.

HTPB must be mixed from its liquid base components, degassed under vacuum, and then cast and cured in a fuel grain mold. HTPB does not melt in the presence of heat, but instead chars and ablates. HTPB burn properties can vary dramatically depending on the curative mix ratio, relative humidity, cure temperature, degree of residual gas seeding in the cast material, and the length of time the material has cured. Typical cure times can vary from 10 days to two weeks. Because HTPB is a thermosetting material, it cannot be shaped and manufactured using FDM methods. Once cast, the HTPB grain cannot be reshaped, reused, or recycled.

Alternatively, the material of choice for FDM manufacturing, acrylonitrile-butadiene-styrene (ABS), is an inexpensive, recyclable thermoplastic that melts at a relatively low temperature, 250°C. This melting point can be precisely controlled and allows ABS to be reshaped and recycled multiple times with little or no degradation of

the material properties. This material is widely mass produced for a variety of noncombustion applications, including household plumbing and structural materials. More than 1.4 billion kilograms of ABS material were produced by petrochemical industries worldwide in 2010 [3].

ABS has several mechanical properties that make it very attractive as a potential hybrid rocket fuel. Because ABS can be formed into a wide variety of shapes using modern additive manufacturing and rapid-prototyping techniques, it is possible to embed complex high-surface area flowpaths within the fuel grain [4]. These internal flowpaths can open up during a burn and allow for motor aspect ratios that are significantly shorter than can be achieved using conventional motor-casting technologies. These embedded flowpaths cannot be achieved with HTPB grains that are cast around mandrels and tooling that must be removed once the material is set.

When subjected to heat, ABS melts before vaporizing, and this liquid-film layer has the effect of providing a significant amount of film cooling along the burning surface. This insulating film layer directs the heat of combustion toward the nozzle exit and allows the external motor case to remain cool during the burn. This self-cooling property of ABS presents a very significant advantage for in-space applications where thermal management becomes a big issue.

Karabeyoglu et al. [5] have noted that, when thermoplastic materials are burned, liquid fuel droplets can be entrained into the oxidizer flow stream, and they may serve to increase the overall regression rate of the propellant. Under certain mechanical conditions, these entrained propellant droplets may also serve to damp both nonacoustic and acoustic flow instabilities in the combustion chamber [6].

Finally, ABS has a very high structural modulus (2.3 GPa) and tensile yield strength (40 MPa). This yield strength is approximately 38% of aluminum. In any design consideration, the relative strength and insulation properties of the ABS seeding material will allow the fuel grain to take a significant portion of the combustion chamber pressure load and reduces the wall thickness requirements. Because ABS is structurally strong and self-insulating, potentially the entire combustion chamber can be fabricated of the ABS fuel material.

To date, however, no detailed analyses of the combustion and thermodynamic performance of ABS as a rocket fuel have been published in the open literature. Because of the preceding properties, if ABS can be demonstrated to be thermodynamically competitive with HTPB, it would represent a very attractive alternative option as a hybrid rocket fuel grain material. Thus characterizing and comparing the regression rates of ABS and HTPB for similar fuel grain geometries and oxidizer flux values was a major goal of this project. This paper details the rocket-based combustion of readily available industrial formulations of ABS with nitrous oxide (N₂O), and compares the performance against HTPB as a baseline. Both analytical predictions and experimental comparisons are presented.

III. Chemical Analysis of Hydroxyl-Terminated Polybutadiene and Acrylonitrilebutadiene-Styrene

Because ABS is widely used as an industrial and domestic construction material, the heat of combustion ΔQ_c in the presence of oxygen has been documented for safety considerations [7]. However, because ABS has not previously been purposely considered as a rocket fuel grain material, there has been little to no published data quantifying the material’s standard enthalpy of formation ΔH_f^0 . The enthalpy of formation is required to calculate the properties of the combustion products when ABS is burned in the presence of nitrous oxide at various mixture ratios and combustion pressures. It is expected that the ABS enthalpy of formation and combustion properties will vary widely depending on the ratio of the various monomers that make up the ABS polymer.

A. Group Addition Method for Calculating the ΔH_f^0 of Polymers

Because of the relative degree of uncertainty regarding the enthalpy of formation of ABS, this study employs a systematic approach for calculating ΔH_f^0 using the “group addition” method developed by Van Krevelen and Jijenhuis [8] and Krevelen and

Table 1 Enthalpy of formation contributions of butadiene and hydroxyl units for an $N = 50$ polymerization of HTPB

Monomer	ΔH_f monomer kJ/g · mol	ΔQ_f polymerization kJ/g · mol	ΔH_f polymer kJ/g · mol	HTPB mole fraction	Enthalpy contribution kJ/g · mol
1, 4 butadiene	104.10 [8]	72.10 [13,16]	32.00	0.9615	30.768
OH	-176.0[8]	— —	-176.00	0.0385	-6.776
HTPB total					23.99

Chermin [9]. Van Krevelen and Jijenhuis's method [8] calculates the Gibbs free energy of formation ΔG_f of a polymer in a gaseous state by summing individual group contributions of common polymer-building molecular groups. Because the Gibbs free energy of a polymer can be estimated as the summed contributions of the individual molecular group's enthalpies of formation minus the contributions of entropy/temperature product, it follows that the enthalpy of formation of the polymer is simply the summation of the contributions of the individual groups to the enthalpy of formation.

B. Calculating ΔH_f^0 for Hydroxyl-Terminated Polybutadiene

The enthalpies of formation of HTPB have been previously published and can vary widely as the relative degrees of polymerization and curative treatments for the mix are modified [10–12]. To verify applicability of the group addition process for rocket combustion, the method described in the preceding paragraph was used to calculate the enthalpy of formation of HTPB. Because HTPB with nitrous oxide as the oxidizing agent is the most commonly used hybrid rocket propellant combination, a large database of performance data exists and can be used to verify the additive group calculations. As an introduction to the group addition method, a detailed calculation for HTPB will be presented here.

A common polymer formulation of HTPB (ARCO R-45M® [13]) has 50 repeating 1,4 butadiene units with a hydroxyl group (OH) terminating each end of the molecule [14]. Van Krevelen and Jijenhuis [8] state the enthalpy of formation for the butadiene monomer as 104.1 kJ/g · mol, and the corresponding heat of polymerization is 71.10 kJ/g · mol [15]. Thus, the total heat contribution of each 1,4 butadiene unit is 32.0 kJ/g · mol. Van Krevelen and Jijenhuis state the enthalpy of formation for each hydroxyl group as -176 kJ/g · mol. For $N = 50$ polymerization, the corresponding mole fractions are 0.9615% for 1,4 butadiene and 0.0385 for the OH group. The total molecular enthalpy of formation for HTPB $\Delta H_{f,HTPB}^0$ is 23.99 kJ/g · mol [16] and the corresponding "reduced" chemical formula is $C_{3.8462}H_{5.8077}N_{0.0385}$. Using this molecular formula, the molecular weight is calculated to be 52.58 kg/kg · mol and the enthalpy of formation in mass units is calculated to be 456.5 kJ/kg. Table 1 summarizes this calculation.

The calculated enthalpy of formation and reduced molecular formula for HTPB neglect the chemical contributions of the isocyanate curing agent used to polymerize and set the material. The curing agent, typically a small fraction of the mixed material (around 12% by mass [17]) is volatile and evaporates from the mix as the material cures. For the final cured and degassed material, the contribution of the curative to the ΔH_f^0 is considered negligible.

C. Thermodynamic and Transport Properties of HTPB/Nitrous Oxide Combustion

The NASA computer program Chemical Equilibrium with Applications (CEA) [18] was used to calculate thermodynamic and transport properties of the products of combustion of HTPB and nitrous oxide. Calculated parameters included adiabatic flame temperature T_0 , ratio of specific heats γ , molecular weight M_w , characteristic velocity c^* , dynamic viscosity μ , and Prandtl number P_r . The CEA code has extensive internal libraries for reactant thermodynamic and transport properties including standard and nonstandard temperature and pressure conditions. Oddly, the CEA thermochemical database does not have an entry for any of the polymerized formulations of HTPB, and the value of ΔH_f^0 and reduced molecular formula calculated in the preceding section must be externally input to the program.

Figure 1 plots the calculated adiabatic flame temperature and characteristic velocity as a function of oxidizer-to-fuel (O/F) ratio and the combustion chamber pressure. Depending on the chamber pressure, the peak c^* performance occurs at an O/F ratio between 5.5 and 6.1. At 7000 kPa chamber pressure (1000 psi), the peak c^* value is 1630 m/s and agrees closely with the "textbook" optimum of 1625 m/s for hybrid HTPB/N₂O combustion [10] and supports the group-addition calculation for the enthalpy of formation. Fortunately, the calculated value of c^* is reasonably insensitive to the input value for the enthalpy of formation for HTPB. A 10% variation in the input ΔH_f^0 produces a 2–3% variation of the peak c^* value and the optimal values for c^* occur at nearly identical O/F ratios.

D. Calculating the ΔH_f^0 of ABS for a Standard Structural Polymer Formulation

The monomers that make up any ABS thermoplastic are 1) acrylonitrile, 2) butadiene, and 3) styrene. Typical, readily available industrial formulations of ABS consist of approximately 50% mole fraction of butadiene, 43% acrylonitrile, and 7% styrene [3], and the reduced chemical formula corresponding to this mix ratio is $C_{3.85}H_{4.85}N_{0.43}$. The molecular weight is calculated to be 57.07 kg/kg · mol. Table 2 shows the individual monomer ΔH_f^0 , heats of polymerization ΔQ_f , the corresponding polymer ΔH_f^0 , constituent mole fractions, and enthalpy contributions of the ABS constituent monomers using the group addition method. Data from presented in Table 2 were obtained from Van Krevelin and Jijenhuis [8], Seymour and Carraher [15], Prosen et al. [16], Baxendale and Madaras [19], and Prosen and Rossini [20]. The enthalpy of formation is calculated as 62.63 kJ/g · mol. The equivalent mass-based enthalpy of formation is 1097.4 kJ/kg. This value is roughly 140% higher than the enthalpy of formation calculated for HTPB. The higher positive

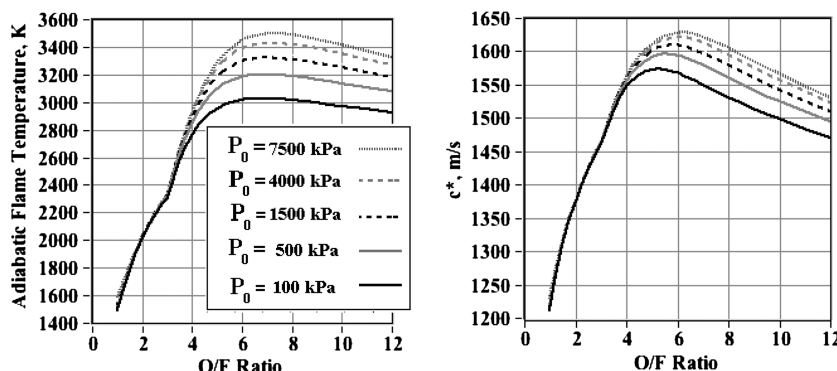


Fig. 1 Thermodynamic and transport properties of N₂O/HTPB combustion products.

Table 2 Enthalpy of formation contributions of acrylonitrile, butadiene, and styrene copolymers in a 50%/43%/07% ABS formulation

Monomer	ΔH_f monomer kJ/g · mol	ΔQ_f polymerization kJ/g · mol	ΔH_f polymer kJ/g · mol	ABSmole fraction	Enthalpy contribution kJ/g · mol
Acrylonitrile	172.62 [19]	74.31 [15]	98.31	0.43	42.27
Butadiene	104.10 [8]	72.10 [16]	32.00	0.50	16.00
Styrene	146.91 [20]	84.60 [15]	63.31	0.07	4.36
ABS total					62.63

calculated enthalpy of formation indicates that this ABS formulation will likely not burn as hot as will HTPB for the same O/F ratio.

Although the authors recognize that the monomer ratio may not produce a propellant with optimal energy content, the ready availability of this stock product favored this formulation for analysis and testing during this phase of the project. The effects of different ABS monomer ratios will be presented later in Sec. VI of this paper.

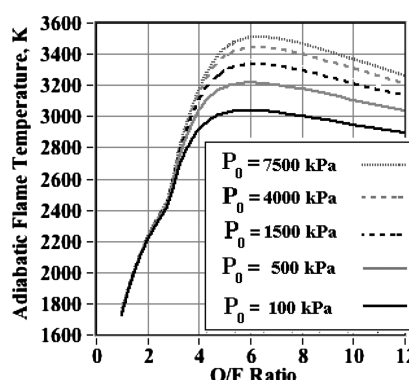
E. Thermodynamic and Transport Properties for ABS/N₂O Combustion

The value of ΔH_f^0 calculated in Table 2 and the corresponding chemical formula were input to CEA to calculate the thermodynamic and transport properties for ABS/N₂O combustion as a function of combustion pressure and O/F ratio. As with HTPB, the CEA-calculated parameters include T_0 , γ , M_w , c^* , μ , and P_r . Figure 2 plots adiabatic flame temperature and characteristic velocity for ABS/N₂O as function of O/F ratio and combustion pressure. When the ABS/N₂O thermodynamic and transport charts are compared against the corresponding HTPB/N₂O charts, two key features are noted: 1) the predicted ABS c^* is lower by slightly less than 1%, and 2) peak c^* values tend to occur at lower O/F ratios (between 4.0 and 5.5). This “optimal point” is significantly lower than the corresponding HTPB O/F optimal values that lie between 5.0 and 6.0. Thus, slightly lower ABS-motor oxidizer flow levels should produce equivalent performance when compared with the HTPB motor. Similar to the HTPB model, a sensitivity analysis for the ABS indicates that a 10% variation in the input ΔH_f^0 produces only a 2–3% variation of the peak c^* value.

IV. End-to-End Motor Performance Modeling

The motor models presented here will be compared against motor burn data from static-fire tests to be described later in Sec. VI. The motor modeling equations are derived from an enthalpy-balance regression rate model adjusted for nonunity Prandtl number of the combustion product. Assuming the nozzle throat chokes immediately, a balance between the gases coming into the fuel port and the gases leaving through the choked throat determines the time response of this chamber pressure growth. Here the equation that describes the time evolution of the chamber pressure is

$$\frac{\partial P_0}{\partial t} = \frac{A_{\text{burn}}}{V_c} [\rho_{\text{fuel}} R_g T_0 - P_0] - P_0 \left[\frac{A^*}{V_c} \sqrt{\gamma R_g T_0 \left(\frac{2}{\gamma + 1} \right)^{\frac{\gamma+1}{\gamma-1}}} \right] + \frac{R_g T_0}{V_c} A_{\text{ox}} C_{d_{\text{ox}}} \sqrt{2\rho_{\text{ox}}(P_{\text{ox}} - P_0)} \quad (1)$$



The oxidizer mass flow rate is modeled by the incompressible discharge coefficient formula

$$\dot{m}_{\text{ox}} = A_{\text{ox}} C_{d_{\text{ox}}} \sqrt{2\rho_{\text{ox}}(P_{\text{ox}} - P_o)} \quad (2)$$

Equation (2) is reasonably accurate as long as the motor is burned using a “top pressure,” that is, higher than the saturation pressure of the N₂O at the injector temperature. For “blowdown” systems that use only the natural vapor pressure of the propellant, a more complicated two-phase model is required to accurately model the injector mass flow [21]. The fuel grain mass flow is modeled as

$$\dot{m}_{\text{fuel}} = A_{\text{burn}} \cdot \rho_{\text{fuel}} \cdot \dot{r} \quad (3)$$

where \dot{r} is the linear fuel regression rate and ρ_{fuel} is the material density of the solid fuel grain. The propellant O/F ratio, which varies significantly throughout the burn, is given by

$$\text{O/F} = \frac{\dot{m}_{\text{ox}}}{\dot{m}_{\text{fuel}}} = \frac{A_{\text{ox}} C_{d_{\text{ox}}} \sqrt{2\rho_{\text{ox}}(P_{\text{ox}} - P_0)}}{A_{\text{burn}} \cdot \rho_{\text{fuel}} \cdot \dot{r}} \quad (4)$$

Modeling the mixture ratio in this form allows calculation of combustion product properties at every time step using a table lookup of the equilibrium exhaust gas properties.

The unique element of the hybrid motor model used here is the fuel grain regression rate equation, developed by Eilers and Whitmore [22] and corrected by Whitmore and Chandler [21] for nonunity Prandtl number

$$\dot{r} = \frac{0.047}{\rho_{\text{fuel}} \cdot Pr^{0.153}} \left(\frac{C_p [T_0 - T_{\text{fuel}}]}{h_v} \right)^{0.23} \left[\frac{A_{\text{ox}} C_{d_{\text{ox}}} \sqrt{2\rho_{\text{ox}}(P_{\text{ox}} - P_0)}}{A_c} \right]^{\frac{4}{5}} \left(\frac{\mu}{L} \right)^{\frac{1}{5}} \quad (5)$$

In Eq. (5), the parameters μ and P_r refer to the combustion product gas properties, the parameters P_{ox} and ρ_{ox} refer to the oxidizer liquid properties upstream of the injector, and C_p , ρ_{fuel} , T_{fuel} and h_v refer to the properties of the solid fuel grain. Equation (5) was developed from an enthalpy balance between the latent heat of the burning fuel and the heat convection into the combustion flame zone. Applying the generalized (nonunity Prandtl number) form of the Reynolds analogy between the Stanton number and the surface skin-friction coefficient allows the heat transfer coefficient to be calculated.

Equations (1–5) are continuously integrated to calculate the chamber conditions and, at each time frame, the chamber properties are used with standard one-dimensional De Laval flow formulas [23]

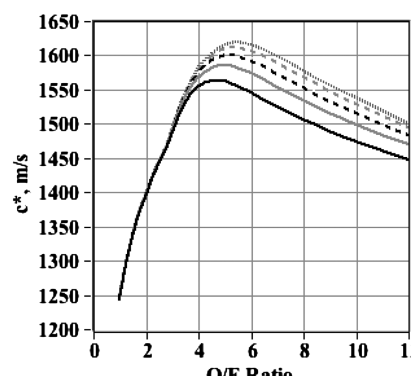


Fig. 2 Thermodynamic and transport properties of N₂O/ABS combustion products.

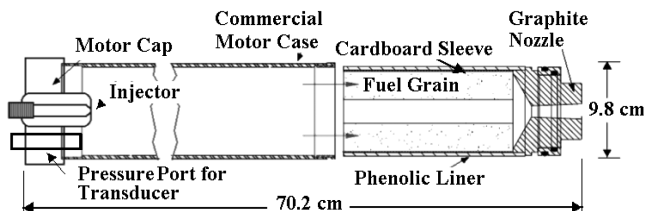


Fig. 3 Cesaroni Pro-98 motor case adapted for hybrid-motor tests.

to calculate the end-to-end rocket performance. Calculated parameters include thrust, exit properties, specific impulse, and choking mass flow. Adjustments are made for nonzero nozzle exit angles and heat loss within the combustor. Nozzle throat dimensions are allowed to erode at prescribed rates.

V. Experimental Setup for HTPB and ABS Fuel Grain Static-Fire Tests

A primary emphasis of this project is the experimental evaluation of FDM-manufactured ABS hybrid fuel grains and performance comparisons to geometrically identical fuel grains cast from HTPB. To achieve this objective, multiple, identically sized HTPB and ABS fuel grains were static fired in a test cell housed on the Utah State University campus. This section details the hybrid motor case design and assembly, fuel grain fabrication methods, test cell instrumentation, and test procedures. Tests results and model comparisons will be presented in Sec. VI.

A. Motor Case, Injector, Nozzle, and Igniter Assembly

Figure 3 shows the original commercially available Cesaroni solid-rocket 98 mm motor[‡] case adapted for these hybrid motor tests. The motor was converted for hybrid testing by replacing the original ejection charge on the motor cap with a single oxidizer injector port. Two small (10 g) Estes-class solid-rocket motors were also inserted into threaded taps on the injector cap. These small motors serve as igniters for the larger hybrid motor. Electronic matches (e-matches) burned by a 12 V dc signal initiated these small motors. The motors and e-matches were replaced after each test firing. To sense chamber pressure, a port was also installed in the modified motor injector cap. A small section of steel tubing transmitted the chamber pressure to the transducer to eliminate the affects of motor heating on the chamber pressure measurement.

To reduce run-to-run variability due to nozzle erosion, nozzles fabricated from a single piece of graphite replaced the original manufacturer-supplied phenolic nozzle. The nozzle was designed to have a 4.2:1 expansion ratio and had a design throat diameter of 1.7 cm. This expansion ratio was optimized for the altitude of the test site at Logan, Utah, approximately 1.47 km above mean sea level. The entire system is reusable, with motor grain cartridges being inserted from the nozzle end of the combustion chamber. Advantages of this configuration design include a ready-made “flight-weight” motor and the ability to rapidly reload fuel grains between motor tests. Table 3 summarizes the motor, nozzle, injector, and fuel grain dimensions.

B. ABS Fuel Grain Fabrication and Test Grain Geometry

Multiple cylindrical ABS fuel grains were fabricated using a Stratasys Fortus®[§] FDM system that is typically used for medium-scale three-dimensional modeling and rapid prototyping. The Stratasys FDM systems use production-grade thermoplastic materials that are sufficiently rugged for functional testing and end-use parts. Real production thermoplastics are stable and have no appreciable warping, shrinkage, or moisture absorption. The stock material used for these tests, Stratasys ABS-M30®, approximates the 50:43:7 monomer ratios analyzed earlier in Sec. V.A. The mean

Table 3 Motor case, nozzle, injector, and fuel grain dimensions

Motor case	70.2 cm length	98 mm diameter	
Nozzle	2.21 cm ² throat area (1.64 cm diam)	9.27 cm ² exit area (3.44 cm diam)	4.2 expansion ratio
Injector	0.115 cm ² exit area (0.383 cm diam)	0.40 discharge coefficient $C_{d,ox}$	—
Fuel grain	57.1.5 cm length	82.6 cm diam	5.07 cm ² port area

density of the FDM-manufactured ABS material used for these tests was approximately 975 kg/m³. The latent heat of gasification h_v , is approximately 2.3 MJ/kg [24].

The fuel grain was fabricated to fit snugly into the motor case described in the preceding section. A postcombustion chamber was premanufactured into the fuel grain. Each fuel grain was approximately 57.15 cm in length, 8.26 cm in diameter, the initial fuel port diameter was 2.54 cm, and postcombustion chambers were 5.66 cm in diameter and 1.27 cm deep. The mean ABS fuel grain weight was approximately 2.67 kg.

The injector port was designed to protrude approximately 1 cm into the top of the fuel grain to eliminate impingement erosion on the upper fuel section and reduce the chances of initiating chaotic or unpredictable burning down the rest of the length of the motor. Each fuel grain is bonded into a cardboard sleeve using high-temperature silicone adhesive. This sleeve is inserted into a phenolic insulating liner, and then into the aluminum motor casing. The nozzle and motor cap assemblies are seated with O-rings. The aluminum motor case acts as the pressure vessel for the motor. Figure 4 presents the fuel images showing the grain features with the major dimensions labeled.

C. HTPB Fuel Grain Fabrication and Test Geometry

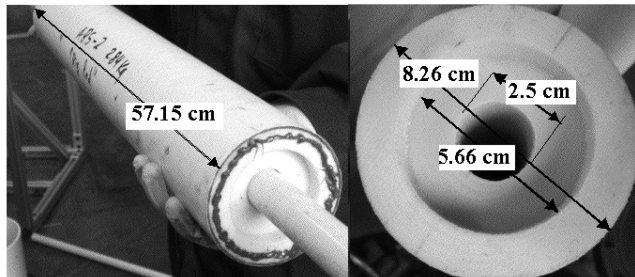
As mentioned earlier in this paper, HTPB fuel grains were cast using the commercially available Arco R45M polybutadiene resin and PAPI 94® MDI curative. Arco R45M is polybutadiene diol manufactured by the Sinclair Petrochemicals Arco Division. The uncured resin has a polymerization factor of approximately 50 and a molecular weight of 2734 kg/kg · mol. PAPI 94 is a polymethylene polyphenylisocyanate produced by Dow® Plastics, Inc. The formulation contains MDI in proprietary proportions. The curative has an average molecular weight of 290 kg/kg · mol. The MDI nitrogen, carbon, oxygen (N-C-O) bonds react with the OH terminations in the polybutadiene resin to cure the fuel grain. For these tests, activated charcoal was added to the mixture to insure opaqueness and prevent radiative heating of the fuel grain and motor case liners. HTPB/MDI/charcoal mass proportions were set at 87/12.5/0.5%, respectively. Past experience has determined that these proportions assure adequate fuel grain cure and material hardness.[¶] As described earlier, the curative is volatile, and its effect on the thermodynamic and transport properties of the products or combustion was considered negligible. Similarly, modeling the charcoal additive in CEA also had little effect on the thermodynamic and transport properties of the combustion products.

The resin and curative were mixed in a commercial paint mixer that was sealed and fitted so that the fuel mixture could be placed under a vacuum during the mixing process. A commercial heating, ventilation, and air conditioning vacuum pump was used to remove gas bubbles created in the fuel grain during the mixing process. The degassed mixture was cast in the same cardboard sleeves used for the ABS fuel grains with a 2.54 cm (1 in.) polyvinyl chloride pipe used as the fuel port mandrel. Before casting, the mandrel was coated with a mold release agent to insure proper release after the fuel grain cured. The HTPB fuel grain dimensions, including the postcombustion chamber, were identical to the previously described ABS fuel grains. The cast fuel grains had a mean mass of 2.55 kg and a mean density of

[‡]Data available online at http://www.pro38.com/pdfs/Pro98_Instructions.pdf [retrieved 13 November 2010].

[§]Data available online at <http://www.fortus.com> [retrieved 15 June 2011].

[¶]Data available online at <http://www.aeroconsystems.com/misc/htpb.htm> [retrieved 14 June 2007].



a) ABS grain installed in liner b) Postcombustion chamber
Fig. 4 ABS fuel grain dimensions.

approximately 930 kg/m^3 . The latent heat of gasification h_v is approximately 1.8 MJ/kg [25].

After casting, the HTPB fuel grains were heat cured and the hardness was continuously monitored throughout the cure process. The HTPB fuel grains took as many as 15 days to reach their final hardness levels. Burning an HTPB fuel grain before it fully cures can produce unpredictable ablation rates and may cause significant chaotic or erosive burning. Chaotic burning produces deep pitting and channeling along the length of the fuel grain and poses a significant burn-through hazard to the motor. Chaotic burning also contributes to a large motor-to-motor thrust and impulse burn-profile variability.

D. Test Cell Apparatus and Instrumentation

As mentioned earlier, an existing test cell at Utah State University was used to perform the motor characterization tests. Measurements obtained include chamber pressure, thrust, total impulse, motor case temperatures, exhaust plume temperatures, specific impulse, mass flow rate, consumed propellant mass, and propellant regression rate. Following each motor test, the fuel grains were dissected and visually inspected for erosive burning and structural failure. Representative fuel grain images will be presented in Sec. VI. All tests results will be compared with analytical predictions.

1. Hybrid Test Stand Oxidizer Delivery System

To allow sufficient mass flow rates with minimal line losses, a predetermined mass of N_2O oxidizer was delivered to a closely coupled “run tank” from a series of K-sized industrial pressure cylinders. In the initial design, the run tank was pressurized by gaseous N_2 to insure a constant injector pressure during the entire length of the burn. During initial system verification and cold flow tests, gaseous nitrogen from the pressurizing tanks was forced into the nitrous oxide storage tanks during the process of supercharging and filling the run tank. This nitrogen gas became dissolved in the stored nitrous oxide and reduced the effectiveness of the oxidizer. Nitrogen was subsequently replaced by helium (He) as the pressurizing fluid. Helium does not readily dissolve and remain in solution in nitrous oxide.

The He supercharge or top pressure was set by a manual regulator and was typically maintained near 5200 kPa (800 psi) for these tests. The top pressure kept the N_2O above saturation pressure for the entire run and insured a single-phase liquid flow through the injector. The run tank volume is approximately 50 liters. A typical run would prefill the tank with only sufficient oxidizer to complete the planned burn time. The design motor chamber pressure was approximately 3440 kPa (500 psi). The pneumatic run valve was triggered by an

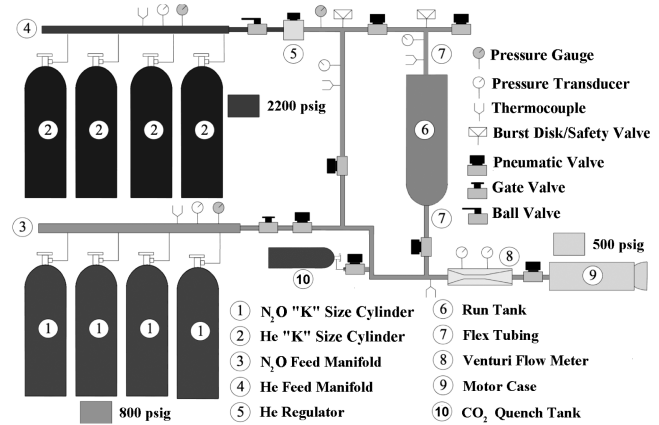


Fig. 5 Oxidizer piping and instrumentation diagram for hybrid motor tests.

electronic relay and was automatically controlled by the instrumentation software. Oxidizer mass flow was sensed by vertical load cells mounted on the run tank and by an inline Venturi flow meter mounted in the oxidizer feed line just ahead of the injector. Figure 5 shows the piping and instrumentation diagram for the hybrid motor test arrangement.

2. Hybrid Test Stand Thrust Balance

The six-degree-of-freedom thrust stand developed for this project provides real-time vertical (motor mass) and axial load (thrust) measurements. Originally a total of six load cells were installed on ball-joint mounts to reduce axial cross coupling. The six-load cells allowed all load paths to be identified. For this series of tests, only the axial and vertical loads were of primary interest. To reduce vibration during the static load tests, the lateral load cells were replaced with clevis support rods mounted on ball shafts.

The axial load was sensed by an Omegadyne® LCCD-500 (2225 N) load cell, and the vertical loads were sensed by two Omegadyne LCCA-25 (110 N) load cells. The output response for these sensors is 3 mV/V , and the sensors were excited using a 12 V dc power source. Chamber pressure was sensed using an MSI®-600 (0–6900 kPa) absolute pressure transducer, closely coupled by steel tubing to the motor cap. Omegadyne type-K thermocouples were mounted at the aft end of the motor case to sense burn temperature and thermal soak-back following the end of the burn. For the latter tests, Omegadyne tungsten-rhenium type-C very high-temperature (3000 K) thermocouples were installed to obtain plume exit temperature measurements. These single-use sensors were very expensive and were used to obtain plume temperatures for only one HTPB and one ABS motor burn. Table 4 lists the manufacturer's specifications, including operating range and accuracy for each of these instruments. The final column of Table 4 lists the installed accuracy of the measurements. These accuracies were evaluated using a series of calibration tests that were performed using control inputs. Installed thrust stand axial and vertical loads were calibrated using the method of Schaeffermeyer et al. [26].

Two National Instruments (NI) data acquisition and control devices managed motor fire control and logged test data. An NI-compact DAQ® four-slot bus controller with multiple analog input (16 bit), analog output, digital output, and thermocouple modules (24 bit) bus cards managed the majority of the measurements and

Table 4 Manufacturer specifications for static thrust stand instruments

Instrument model	Operating range	Manufacturer specified accuracy	Installed measurement accuracy
LCCA-25 (vertical loads)	$\pm 25 \text{ lbf}$ (110 N)	$\pm 0.37\%$ of full scale	side load, $\pm 0.1 \text{ lbf}$ (0.41 N)
LCCD-500 (axial loads)	$\pm 500 \text{ lbf}$ (2225 N)	$\pm 0.25\%$ of full scale	axial load, $\pm 1.45 \text{ lbf}$ (0.651 N)
MSI-600 (chamber pressure)	0–1000 psia (0–6900 kPa)	$\pm 0.1\%$ of full scale	$\pm 1.5 \text{ Psi}$ (10 kPa)
Omega type-K thermocouple (motor case)	95–1500 K	$\pm 2.2^\circ \text{C}$	$\pm 2^\circ \text{C}$
Omega type-C thermocouple (nozzle exit plume)	1650–3000 K	$\pm 0.5\%$ of reading	$\pm 15^\circ \text{C}$

valve control. The digital outputs from a separate NI USB-6009® module were used to trigger the relays that fired the igniter e-matches. Operators and experimenters were remotely located in a secure control room separated from the test area. Communications to the test stand were managed by an operator-controlled laptop via universal serial bus using amplified extension cables. All control and measurement functions were controlled by a LABview® program hosted on the control laptop. Figure 6 presents a schematic of the test stand and an image of the motor being fired. The type-C thermocouple is shown mounted in the nozzle exit plume.

VI. Results and Discussion

To date, more than 40 successful static tests of FDM-fabricated ABS and traditionally cast HTPB fuel grains have been performed. Burn profiles from representative tests for both the HTPB and ABS fuel grains will be presented here. Postburn fuel grain images and total-fuel linear-regression data will also be presented. Finally, test results will be compared with model predictions.

A. Thrust Stand Time History Data

Figure 7 presents side-by-side comparisons of the thrust and chamber pressure time history data collected from six representative HTPB and ABS static firings. For these tests, an identical regulated supercharge or top pressure was used. The regulator setting was verified before each test. During all of these test runs, the steady-state oxidizer mass flow (as measured by the inline Venturi system) remained essentially constant. The burn time was preprogrammed with each burn lasting approximately 10 s. At the end of the prescribed burn time, the oxidizer flow valve was shut off and the motor was quenched using CO₂.

On average the HTPB fuel grains delivered a small but consistently higher overall mean thrust and total impulse levels. For the six burn time histories presented, the mean steady-state thrust for the HTPB grains is approximately 836.0 N, and 796.0 N for the ABS grains. The mean 10 s burn total impulse for HTPB fuel grains is 8999.1 N · s, and the total impulse for the ABS grains is 8631.6 N · s. The HTPB grains produced an effective ensemble mean specific impulse of approximately 225.1 s. This value is approximately 4.2% higher than the mean for the ABS fuel grains, which is 215.9 s. The effective specific impulse is calculated by dividing the total impulse generated during the burn by the measured fuel and oxidizer mass consumed. The equivalent vacuum-specific impulse values are 246.7 (HTPB) and 236.9 s (ABS). The vacuum-specific impulse calculation assumes a nozzle exit area of 9.27 cm² and an ambient test pressure of 86 kPa. Clearly, the 4.2:1 expansion ratio is not ideal for in-space applications. If the motors were retrofitted with a high-expansion ratio nozzle, then the expected vacuum I_{sp} values would be significantly higher.

Interestingly, as clearly demonstrated by the time history data presented in Fig. 7, the ABS fuel grains exhibit a greater run-to-run thrust and total impulse consistency when compared with the HTPB fuel grains. The standard deviation in total impulse for the HTPB motor burns is ± 318.7 N · s, whereas the standard deviation in total impulse for the ABS grains is only ± 193.1 N · s, a consistency improvement of better than 49%. The corresponding steady-state thrust variability is ± 26.2 N for the HTPB grains and ± 9.1 N for the ABS grains, a consistency improvement of almost three-to-one.

This improved run-to-run consistency is likely a positive benefit of the FDM manufacturing process used to fabricate the ABS grains. As compared with the labor-intensive mixing, degassing, casting, and curing process for the HTPB fuel grains, FDM is a precisely controlled robotic industrial process. This consistency difference may also be a result of HTPB being a thermosetting material that chars and erodes before gasifying, whereas ABS is a thermoplastic material that melts and then evaporates. Unquestionably, this topic requires further research, but it appears that the digital manufacturing methods demonstrate the potential for enhanced consistency in the fuel grain fabrication process.

B. Fuel Grain Regression Measurements

Following the end of each static test, the motor was quenched and then split longitudinally to expose the burned grain pattern. The final regression dimensions were measured at multiple points along the fuel grain, and the mean end-to-end longitudinal fuel regression was calculated. Figure 8 shows side-by-side comparisons of post-10-s-burn HTPB and ABS fuel grains. The regression measurement stations are marked on each grain. Both the HTPB and ABS grains burned in a linear manner, and little chaotic or erosive burn patterns were noted. For both the HTPB and ABS grains, fossilized surface flow patterns are visible, and the transition from laminar to turbulent flow patterns is clearly visible.

The increased thrust and total impulse for the HTPB fuel grains appear not to be driven by a higher overall propellant mass flow. The mean N₂O oxidizer mass flows for the HTPB and ABS burns are 0.304 and 0.302 kg/s, respectively. The corresponding fuel burn rates are 0.082 (HTPB) and 0.086 kg/s (ABS). The fuel burn rates were calculated by dividing the total consumed fuel by the total burn duration. The total mass flows are essentially identical.

These calculations are further supported by postburn fuel grain regression measurements. Figure 9 plots the longitudinal mean regression-rate measurements of the HTPB and ABS burns against the mean oxidizer mass flux for the burn. These data are compared with the analytical model predictions of Eq. (5). The mean regression rates are calculated using the two of the methods developed by Karabeyoglu et al. [27]: 1) based on the mean longitudinal change in diameter divided by one-half of the burn time,

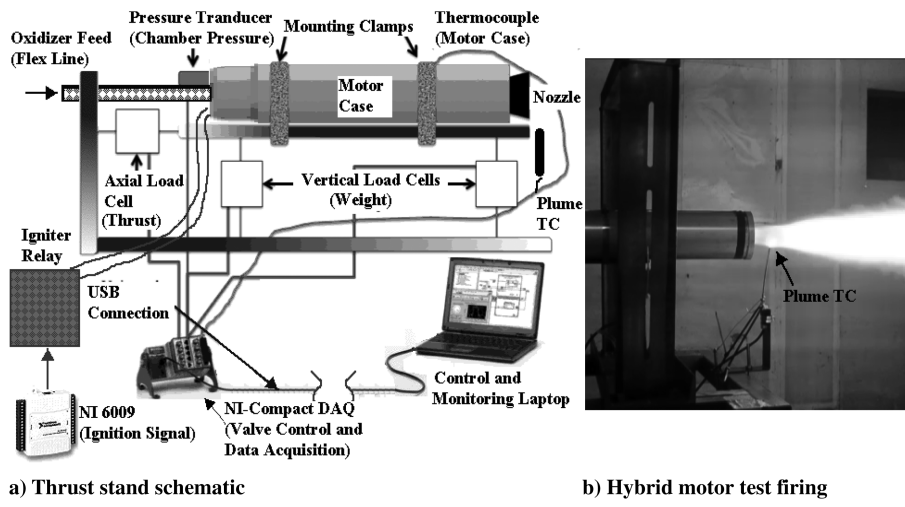


Fig. 6 Static test mechanical and instrumentation schematic.

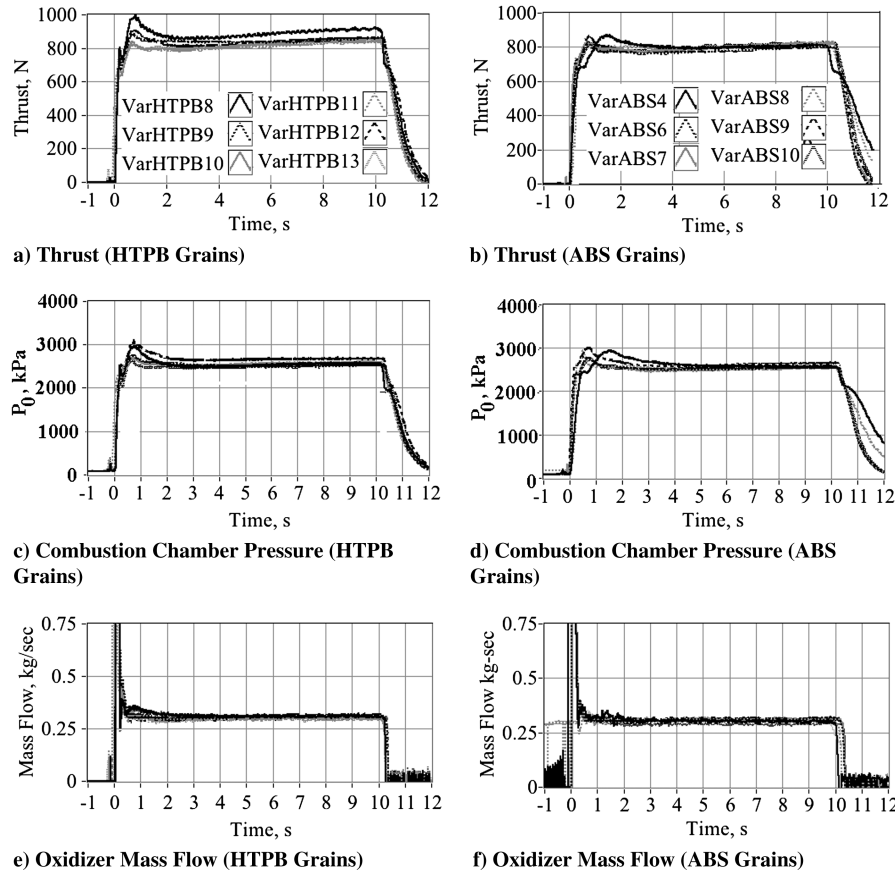


Fig. 7 Thrust, impulse, and mass flow time history comparisons for six representative HTPB and ABS hybrid motors.

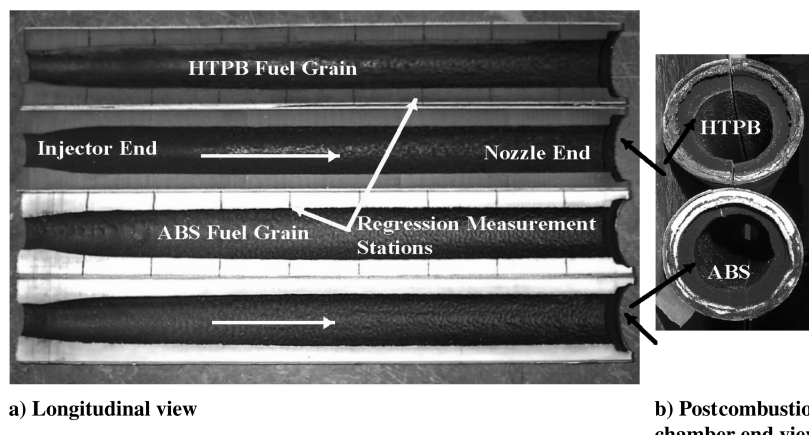


Fig. 8 Burned HTPB and ABS fuel grains.

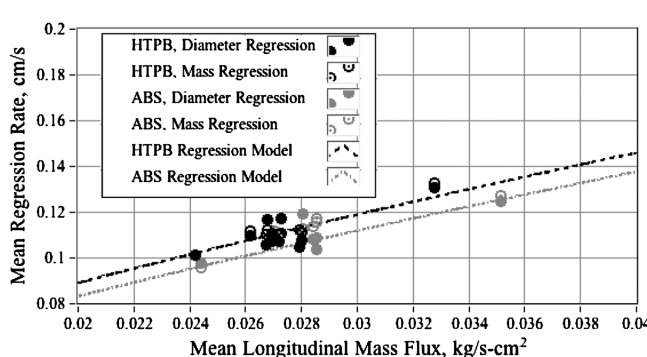


Fig. 9 Predicted and measured linear regression for HTPB and ABS grains.

$$\bar{r}_{\text{dia}} = \frac{\bar{D}_{\text{final}} - D_0}{2 \cdot t_{\text{burn}}} \quad (6)$$

and 2) by the overall change in propellant mass divided by the burn time

$$\begin{aligned} \bar{r}_{\text{mass}} &= \frac{\Delta M_{\text{fuel}} / t_{\text{burn}}}{\pi \cdot \rho_{\text{fuel}} \cdot D_{\text{final}} \cdot L} \\ &= \frac{\Delta M_{\text{fuel}} / t_{\text{burn}}}{\pi \cdot \rho \cdot \sqrt{D_0^2 + (4 \cdot \Delta M_{\text{fuel}} / \pi \cdot \rho_{\text{fuel}} \cdot L)} \cdot L} \end{aligned} \quad (7)$$

The mean oxidizer mass flux is calculated using the mean of the initial and final port diameters

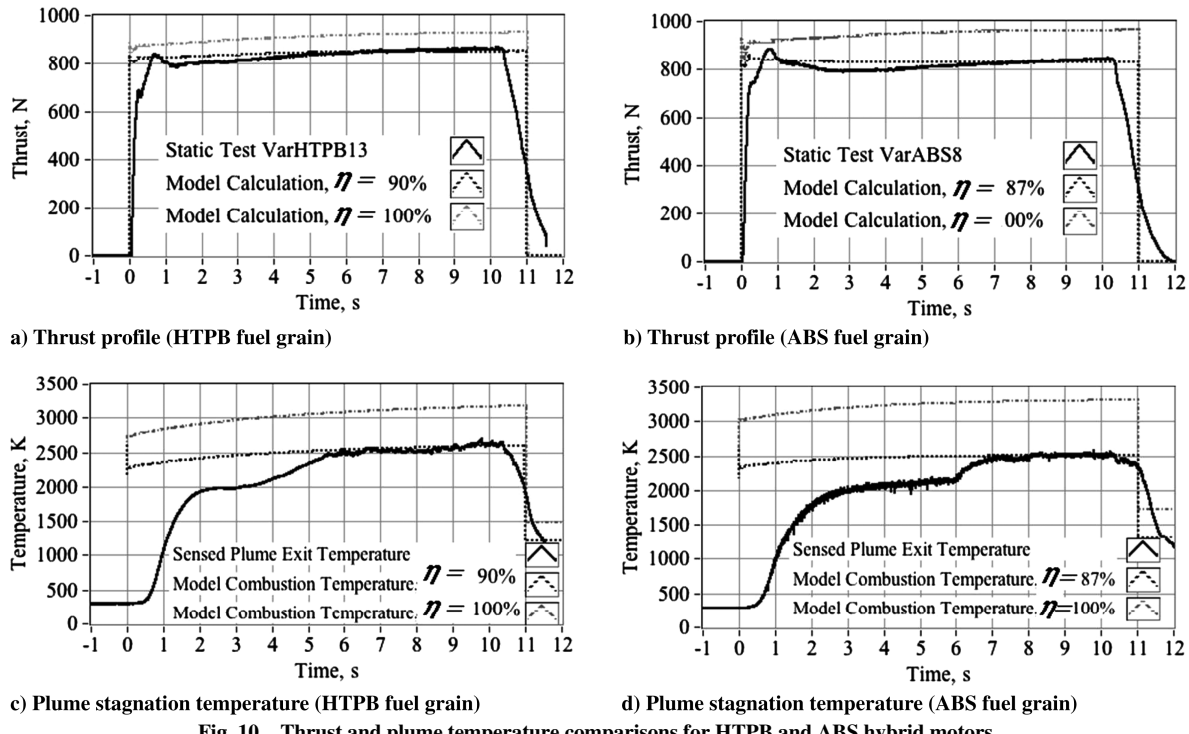


Fig. 10 Thrust and plume temperature comparisons for HTPB and ABS hybrid motors.

$$\bar{G}_{\text{ox}} = \frac{16 \cdot \Delta M_{\text{ox}} / t_{\text{burn}}}{\pi \cdot (D_0^2 + \bar{D}_{\text{final}}^2)} \quad (8)$$

Both the experimental and analytical calculations agree in predicting a slightly higher linear regression rate for HTPB when compared with ABS. However, considering that the ABS material has a slightly higher density (975 kg/m^3) than does HTPB (930 kg/m^3), the resulting solid fuel mass flow at a given oxidizer mass flux is nearly identical for the two fuel materials. Thus, as asserted earlier, it does not appear that differences in propellant mass flows account for the different thrust and impulse levels observed in Fig. 7.

C. Modeled and Sensed Flame Temperature Comparisons

A higher burn temperature for the HTPB fuel grains appears to be the most likely reason for the slightly increased thrust and specific impulse. The combustion efficiency

$$\eta^* = \frac{C_{\text{actual}}^*}{C_{\text{ideal}}^*} = \sqrt{\frac{T_{0_{\text{actual}}}}{T_{0_{\text{ideal}}}}} \quad (9)$$

of the analytical model was adjusted until the predicted flame temperature best matched the plume exit temperature measurements

sensed using very high-temperature type C thermocouples. Figures 10a and 10b plot the HTPB and ABS thrust profiles overlaid against model predictions with $\eta^* = (100 \text{ and } 90\%)$ for the HTPB motor, and against model predictions with $\eta^* = (100 \text{ and } 87\%)$ for the ABS motor. Figures 10c and 10d present the plume temperature time history data compared against the model flame temperature predictions.

Early in each burn profile, the plume thermocouples glowed brightly and experienced considerable radiation temperature loss. As the propellant exhaust products “blackened” the thermocouples, the radiation heat loss from the glowing thermocouple bead was significantly reduced and the sensed temperatures leveled off to approach their peak values. The sensed peak plume stagnation temperatures correspond to 90 and 87% combustion efficiency for HTPB and ABS, respectively. These reduced combustion efficiencies may account for the lower than expected specific impulses presented in Sec. VI.A. When the measured specific impulses are adjusted for measured combustion inefficiencies, the mean test altitude and vacuum I_{sp} values for the HTPB motors are 250.1 and 274.1 s, respectively. For the ABS motor burns, the adjusted I_{sp} values for the ABS motors are 248.2 and 272.3 s, respectively.

The most important point to take away from Figs. 10c and 10d is that the sensed plume temperature for the ABS fuel grain burn is approximately 3.5% lower than for the HTPB fuel grain burn. This lower plume temperature supports the earlier analytical conclusion that the ABS fuel grain burns with a slightly lower energy.

Table 5 Oxygen bomb calorimetry measurements for HTPB and ABS fuel grains

Sample	Fuel grain	Weight, g	Wire length, cm	Initial bomb temp, C	Final bomb temp, C	Consumed wire length, cm	Heat of combustion, ΔQ_c , kJ/kg
1	HTPB	0.307	15.24	22.255	23.551	6.99	42.36
2	HTPB	0.301	15.24	22.396	23.664	5.08	42.30
3	HTPB	0.283	15.24	22.273	23.465	7.37	42.25
4	HTPB	0.28	15.24	23.03	24.22	5.08	42.67
5	HTPB	0.48	15.24	22.07	24.16	5.08	43.64
ABS fuel grain combustion statistics: Mean $\Delta Q_c = 42.64 \pm 0.58 \text{ kJ/kg}$							
1	ABS	15.24	15.24	22.54	23.80	7.62	39.38
2	ABS	0.32	15.24	22.42	23.70	10.80	39.47
3	ABS	0.30	15.24	23.06	24.24	8.89	39.70
4	ABS	0.31	15.24	22.68	23.92	10.16	39.71
5	ABS	0.31	15.24	22.68	23.92	10.16	39.74
ABS fuel grain combustion statistics: Mean $\Delta Q_c = 39.60 \pm 0.16 \text{ kJ/kg}$							

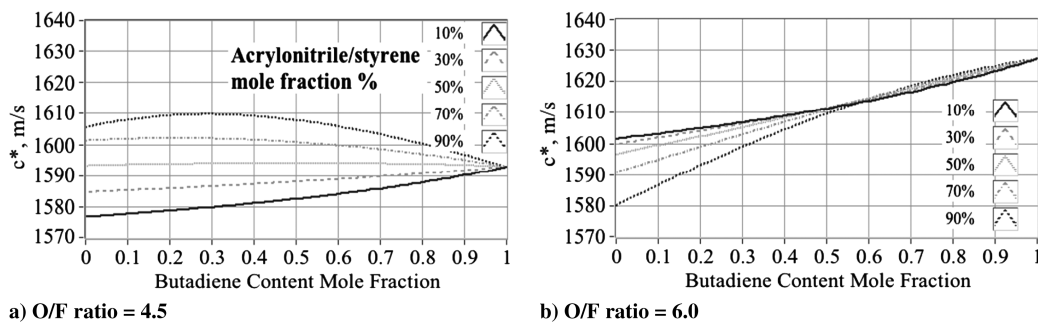


Fig. 11 Affect of ABS monomer mole fractions on combustion performance.

D. Heat of Combustion Calorimetric Measurements for the HTPB and ABS Fuel Grains

A final series of oxygen bomb calorimetry tests were performed on sections of postburn HTPB and ABS fuel grains to add supporting data for the conclusions reached in the preceding sections. Combustion with oxygen in a sealed bomb is a very effective and reliable method for releasing all heat energy obtainable from a sample, and the authors believe that these results verify the higher overall energy content of the HTPB grain formulation when compared with the 50:43:7 ABS formulation evaluated in this project. In this series of tests, a Parr model 1241® oxygen bomb adiabatic calorimeter was used to burn multiple fuel samples selected at random from the burned fuel grains. The gross heat of combustion was measured according to procedures outlined in the American Society for Testing of Materials D2382-88 [28]. Table 5 summarizes these test results. The measured gross heats of combustion for HTPB and ABS agree well with published values [7]. The approximately 7% higher measured heat of combustion for HTPB agrees well with the previously established performance differences.

E. ABS Fuel Grain Monomer Ratio Optimization

As the data presented for the earlier 50:43:7 butadiene/acrylonitrile/styrene monomer mole fraction demonstrated, the energy content of this ABS formulation is slightly but consistently lower than the R-45m HTPB formulation. This final section examines the individual ABS monomer mole fraction ratios to search for an optimal formulation. The mole fractions of each polymer were varied from 0 to 100% of the constituents of the polymer, such that the total makeup of each of the formulations equals 100%. For example, if the first component was 50% of the total constituency, the other two components were varied so that the sums of their mole fractions totaled the other 50%. The group addition method was used to calculate ΔH_f^0 for the various ABS polymerizations, and this data, along with the corresponding molecular formulas, was input into the CEA program for various oxidizer-to-fuel ratios and combustion pressures. The resulting values for the equilibrium species concentrations, thermodynamic properties, and transport properties were used to calculate the propellant's characteristic velocity for each of the possible monomer combinations. The monomer ratios producing the higher c^* values give the more desirable propellant combinations.

Figure 11 plots the characteristic velocity for ABS/N₂O combustion at 2500 kPa chamber pressure as a function of butadiene mole fraction for various remaining acrylonitrile/styrene (A/S) ratios. Calculations for different mixture ratios (O/F = 4.5 and 6.0) are presented. Clearly, for the lower O/F ratio (4.5), there exists an optimal butadiene content that peaks near a 30% total mole fraction and 90% A/S ratio. For lower A/S ratios, this optimal point diminishes. In contrast, for the higher O/F ratio (6.0) there is no optimal point, and increasing butadiene content always leads to a better performing propellant.

For the higher O/F ratio, the propellant performance is more or less independent of the A/S ratio. For a 2500 kPa operating chamber pressure and an O/F ratio of 6.0, 70% butadiene content results in a c^* value of 1618 m/s. That c^* value exceeds the HTPB c^* of 1608 m/s for the same operating pressure and O/F ratio (Fig. 1). At this juncture in the research, it is unclear what allowable fraction of butadiene will

retain adequate structural integrity for the fuel grain material. This analysis suggests that future preparations of ABS may be better optimized for hybrid propellant performance, but also that the mixture that produces best results is closely coupled with the operating O/F ratio of the motor.

VII. Conclusions

A primary objective of this work was to investigate the viability of acrylonitrile-butadiene-styrene (ABS) as a hybrid rocket fuel material. ABS is an inexpensive thermoplastic that can be readily shaped into complex geometries using fused deposition modeling (FDM), a form of direct digital manufacturing. Leveraging the recent rapid capability growth in factory automation and robotics, FDM offers the potential to revolutionize methods used to fabricate hybrid rocket fuel grains and other hybrid rocket components. Once matured and commercialized, this technology will have a transformational effect on hybrid rocket motor production by improving quality, consistency, and performance, while reducing development and production costs.

The performance of ABS thermoplastic is compared with hydroxyl-terminated polybutadiene (HTPB) with N₂O as the matching oxidizer. Multiple ABS grains were FDM fabricated from existing ABS stock materials composed of 50:43:7 butadiene, acrylonitrile, and styrene mole fractions. Static test burn data from the ABS grains were compared against burn data obtained for traditionally cast HTPB grains of equal physical volume and dimension. Test results demonstrate that the ABS fuel grains have an acceptable but slightly reduced performance when compared with HTPB. End-to-end linear regression rate, plume temperature measurements, and bomb calorimetry measurements of the heats of combustion were collected to support the static-fire burn performance data. In all cases the ABS formulation burns with an almost identical mass flow but produces slightly less burn energy than does the HTPB material. Possible sources of this lower burn energy could be the higher heat of gasification for ABS and a higher enthalpy of formation for the stock ABS materials tested for this project.

Another significant conclusion of the static tests is that the ABS fuel grains demonstrated a higher burn-to-burn performance consistency. This improved run-to-run consistency is likely a positive benefit of the FDM additive manufacturing process used to fabricate the ABS grains. FDM manufacturing is precisely controlled by robotic industrial process, as opposed to the labor-intensive mixing, degassing, casting, and curing process for the HTPB fuel grains.

This study concludes with an examination of the effects of relative monomer compositions for the ABS fuel grains. This final section examines the individual ABS monomer mole fraction ratios to search for an optimal formulation. Calculations for different mixture ratios were presented. For the lower oxidizer-to-fuel (O/F) ratio (4.5), there exists an optimal butadiene content that peaks near a 30% total mole fraction and 90% A/S ratio. For the higher O/F ratio (6.0), there is no optimal point, and increasing butadiene content always leads to a better performing propellant. For the higher O/F ratio, 70% butadiene content results in an ABS c^* that exceeds the HTPB c^* for the same operating pressure and O/F ratio.

At this juncture, it is unclear what allowable fraction of butadiene will retain adequate structural integrity for the fuel grain material.

This analysis suggests that future preparations of ABS may be better optimized for hybrid propellant performance, but also that the mixture that produces the best results is closely coupled with the operating O/F ratio of the motor. In all cases, the viability of industrially produced ABS fuel grains has been clearly proven. For this initial study, simple cylindrical port grain configurations were modeled and tested. Future studies will examine digital manufacturing methods for allowing higher burn regression rates and increasing the burn efficiency of the ABS fuel material formulation.

Acknowledgments

This work was partially funded under a grant from the Utah Governor's Office of Economic Development Technology Commercialization and Innovation Program and the NASA Experimental Program for Stimulating Competitive Research. The authors also thank teaming partner Aviradyne Technologies of Layton, Utah for procuring the acrylonitrile-butadiene-styrene fuel grains from Stratasys, Inc.

References

- [1] Robichaud, R., (ed.), "Hazard Analysis of Commercial Space Transportation: Vol. 1, Operations; Vol. 2, Hazards; Vol. 3, Risk Analysis," U.S. Dept. of Transportation, PB93-199040, Accession No. 00620693, May 1988.
- [2] Wright, P. K, *21st Century Manufacturing*, Prentice-Hall, Upper Saddle River, NJ, 2001, pp. 7–67.
- [3] Feldman, J., "Plastics—Materials of the 21st Century," *BASF News Releases*, http://www.bASF.de/bASF2/html/plastics/englisch/pages/presse/04_261.htm [retrieved 13 June 2011].
- [4] Fuller, J. K., Ehrlich, D. A., Lu, P. C., Jansen, R. P., and Hoffman, J. D., "Advantages of Rapid Prototyping for Hybrid Rocket Motor Fuel Grain Fabrication," *47th AIAA/ASME/SAE/ASEE Joint Propulsion Conference & Exhibit*, AIAA Paper 2011-5909, 2011.
- [5] Karabeyoglu, M. A., Altman, D., and Cantwell, B. J., "Combustion of Liquefying Hybrid Propellants: Part 1, General Theory," *Journal of Propulsion and Power*, Vol. 18, No. 3, March 2002, pp. 610–620. doi:10.2514/2.5975
- [6] Blomshield, F. S., "Lessons Learned in Solid Rocket Combustion Instability," *43rd AIAA/ASME/SAE/ASEE Joint Propulsion Conference & Exhibit*, AIAA Paper 2007-5803, 2007.
- [7] Walters, R. N., Hackett, S. M., and Lyon, R. E., "Heats of Combustion of High Temperature Polymers," *Journal of Fire and Materials*, Vol. 24, No. 5, Sept.–Oct. 2000, pp. 245–252. doi: 10.1002/1099-1018(200009/10)24:5<245::AID-FAM744>3.0.CO;2-7
- [8] Van Krevelen, D. W., and Jijenhuis, K., *Properties of Polymers: Their Correlation with Chemical Structure; Their Numerical Estimation and Prediction from Additive Group Contributions*, 4th ed., Elsevier, New York, 2009, pp. 749–761.
- [9] Krevelen, D. V., and Chermín, H., "Estimation of the Free Enthalpy (Gibbs Free Energy) of Formation of Organic Compounds from Group Contributions," *Chemical Engineering Science*, Vol. 1, No. 2, 1951, pp. 66–80. doi: 10.1016/0009-2509(51)85002-4
- [10] Sutton, G. P., and Biblarz, O., *Rocket Propulsion Elements*, 8th ed., Wiley, Hoboken, NJ, 2010, pp. 711–726.
- [11] Ramakrishna, P. A., Paul, P. J., and Mukunda, H. S., "Sandwich Propellant Combustion: Modeling and Experimental Comparison," *Proceedings of the Combustion Institute*, Vol. 29, No. 2, 2002, pp. 2963–2973. doi:10.1016/S1540-7489(02)80362-5
- [12] Rajesh, K. K., "Thrust Modulation in a Nitrous-Oxide/Hydroxyl-Terminated Polybutadiene Hybrid Rocket Motor," *42nd AIAA/ASME/SAE/ASEE Joint Propulsion Conference & Exhibit*, AIAA Paper 2006-4503, 2006.
- [13] Allan, W. D., Baumgartner, W. E., and Meyer, G. E., "HTPB Polymer Improvement," Air Force Rocket Propulsion Lab. (AFRPL) TR-72-89, Sept. 1972.
- [14] Wingborg, N., "Increasing the Tensile Strength of HTPB with Different Isocyanates and Chain Extenders," *Polymer Testing*, Vol. 21, No. 3, 2002, pp. 283–287. doi:10.1016/S0142-9418(01)00083-6
- [15] Seymour, R. B., and Carraher, C. E., Jr., *Polymer Chemistry, Revised and Expanded*, 6th ed., Marcel Dekker, New York, 2003, pp. 291–366.
- [16] Prosen, E. J., Maron, F. W., and Rossini, F. D., "Heats of Combustion, Formation, and Insomerization of Ten C4 Hydrocarbons," *Journal of Research of the National Bureau of Standards*, Vol. 46, No. 1, Jan. 1951, pp. 106–112.
- [17] Kuo, K. K., Lu, Y. C., Chiaverini, M. J., Johnson, D. K., and Risha, G. A., "Fundamental Phenomena on Fuel Decomposition and Boundary-Layer Combustion Processes with Applications to Hybrid Rocket Motors," NASA CR-201643, June 1996.
- [18] Gordon, S., and McBride, B. J., "Computer Program for Calculation of Complex Chemical Equilibrium Compositions and Applications," NASA RP-1311, 1994.
- [19] Baxendale, J. H., and Madaras, G. W., "Kinetics and Heats of Copolymerization of Acrylonitrile and Methyl Methacrylate," *Journal of Polymer Science*, Vol. 19, No. 91, Jan. 1956, pp. 171–179. doi:10.1002/pol.1956.120199117
- [20] Prosen, E. J., and Rossini, F. D., "Heats of Formation and Combustion of 1,3-Butadiene and Styrene," *Journal of Research of the National Bureau of Standards*, Vol. 34, No. 1, Jan. 1945, pp. 59–63.
- [21] Whitmore, S. A., and Chandler, S., "An Engineering Model for Saturated N2O Propellant Feed Systems," *Journal of Propulsion and Power*, Vol. 26, No. 4, 2010, pp. 706–714. doi:10.2514/1.47131
- [22] Eilers, S. D., and Whitmore, S. A., "Correlation of Hybrid Rocket Propellant Regression Measurements with Enthalpy-Balance Model Predictions," *Journal of Spacecraft and Rockets*, Vol. 45, No. 4, Sept.–Aug. 2008, pp. 1010–1020. doi:10.2514/1.33804
- [23] Anderson, J. D. Jr., *Modern Compressible Flow with Historical Perspective*, 3rd ed., McGraw-Hill, New York, 2003, pp. 127–187.
- [24] Panagiotou, J., "A Methodology for Flammability Diagrams," M.S. Thesis, Dept. of Fire Protection Engineering, Univ. of Maryland, College Park, MD, 2004, pp. 10–23.
- [25] Stoliarov, S. I., and Walters, R. N., "Determination of the Heats of Gasification of Polymers Using Differential Scanning Calorimetry," *Polymer Degradation and Stability*, Vol. 93, No. 2, 2008, pp. 422–427.
- [26] Schaeffermeyer, M. R., Whitmore, S. A., and Wright, C. B., "Maneuvering and Gravity Offset Flight Controls for an Extraterrestrial Surface Landing Research Vehicle," *46th AIAA/ASME/SAE/ASEE Joint Propulsion Conference & Exhibit*, AIAA Paper 2010-6936, 2010.
- [27] Karabeyoglu, M. A., Cantwell, B. J., and Zilliac, G., "Development of a Scalable Space-Time Regression Rate Expression for Hybrid Rockets," *41st AIAA/ASME/SAE/ASEE Joint Propulsion Conference & Exhibit*, AIAA Paper 2005-3544, 2005.
- [28] Anon., "D2382-88: Standard Test Method for Heat of Combustion of Hydrocarbon Fuels by Bomb Calorimeter (High Precision Method)," 3rd ed., *ASTM Fire Test Standards*, American Society for Testing of Materials, Philadelphia, 1990, pp. 230–238.

S. Son
Associate Editor